A General Scheme for the Discontinuous Galerkin Time-Domain Modeling and S-Parameter Extraction of Inhomogeneous Waveports

Geng Chen, Lei Zhao, *Member, IEEE*, Wenhua Yu, *Senior Member, IEEE*, Su Yan, *Senior Member, IEEE*, Kedi Zhang, *Member, IEEE*, and Jian-Ming Jin, *Fellow, IEEE*

***Abstract*— A general numerical scheme is proposed for the waveport modeling and scattering-parameter (S-parameter) extraction of inhomogeneous waveports with the discontinuous Galerkin time-domain method. In this scheme, the waveports are truncated with perfectly matched layers with a hybrid mesh automatically extruded from the mesh of the physical device to be simulated. The waveports are then excited by a total-field/scattered-field technique, with which the incident and scattered waves can be obtained for an accurate calculation of the S-parameters. A novel eigenmode solver is also developed to calculate the required modal profiles for the eigenmodes in both homogeneous and inhomogeneous waveports. Special attention is paid to the S-parameter extraction for evanescent modes, which has been a difficult task for time-domain simulations. Numerical examples are given to validate the proposed numerical scheme.**

***Index Terms*— Discontinuous Galerkin time domain (DGTD), S-parameter extraction, total-field/scattered-field (TF/SF) decomposition, waveport modeling.**

I. Introduction

SINCE its development, the discontinuous Galerkin time-domain (DGTD) method [1]–[6] has been applied successfully to a variety of electromagnetic problems, including the modeling and simulation of radio frequency (RF), microwave, millimeter-wave, and optical devices. As most devices are connected to external structures through a port or multiple ports that transmit electromagnetic waves into and/or out of the devices, a critical issue in the device modeling and simulation is to treat these so-called waveports, which includes the truncation of the ports, the excitation of the ports, and the extraction of the scattering-parameters (S-parameters) of the devices. This issue has been investigated extensively in the past two decades, and highly accurate numerical approaches have been developed for the numerical modeling in the frequency domain for any general waveports [7], [8]. For the time-domain modeling, various numerical schemes have also been developed [9]–[19]. The most accurate scheme is to employ a waveport boundary condition (WPBC) [12]–[14], [17], [19] formulated with the eigenmodes of the waveport, which is applicable to homogeneous waveports. This method has been used both in the finite-element time-domain (FETD) and DGTD methods, but only for homogeneous waveport. This happens because for the eigenmodes of a homogeneous waveport, there is an explicit frequency dependence of the wave impedance and propagation constant and the modal profiles are invariant of the frequency. Since such an explicit dependence and invariance do not exist for inhomogeneous waveports, the WPBC cannot be applied directly to the modeling of inhomogeneous waveports. At present, the commonly used approach is to truncate an inhomogeneous waveport using perfectly matched layers (PMLs), excite the port with either a lumped or a distributed current source, and extract the S-parameters by extending the waveports to be simulated so that the incident and reflected waves can be separated.

The objective of this paper is to present a general numerical scheme for an accurate and efficient modeling and S-parameter extraction of inhomogeneous waveports in the DGTD simulation of RF, microwave, millimeter-wave, and optical devices. As was done previously, the waveports are truncated using an uniaxial PML. However, to alleviate the burden associated with the meshing of the PML and enhance the computational efficiency in the PML region, we employ a hybrid mesh consisting of hexahedral and wedge elements directly extruded from the tetrahedral mesh or the mixed mesh of various elements of the physical device to be simulated. As the DGTD mass matrices associated with hexahedral and wedge meshes are either diagonal or block diagonal matrices, the use of a hybrid mesh in the PML region can significantly reduce the memory usage and speed up the computation.

The most important contribution of this paper is to introduce a total-field/scattered-field (TF/SF) method to excite the waveports and extract S-parameters of the device. The TF/SF method has been previously developed for the finite-difference time-domain (FDTD) and FETD methods to model open-region scattering and antenna problems [20], [21]. Its application to the waveport modeling in the DGTD is, however, more involved [22]. To this end, we first introduce a

Manuscript received July 28, 2017; revised November 6, 2017; accepted December 12, 2017. Date of publication January 5, 2018; date of current version April 3, 2018. This work was supported in part by the National Science Foundation of China under Grant 61771226, Grant 61671223, and Grant 61372057 and in part by the Open Project of State Key Laboratory of Millimeter Waves under Grant K201613. *(Corresponding author: Lei Zhao.)*

G. Chen, L. Zhao, and W. Yu are with the Center for Computational Science and Engineering, School of Mathematics and Statistics, Jiangsu Normal University, Xuzhou 22116, China (e-mail: gengchn@163.com; leizhao@jsnu.edu.cn; yuwenhua@jsnu.edu.cn).

S. Yan, K. Zhang, and J.-M. Jin are with the Center for Computational Electromagnetics, Department of Electrical and Computer Engineering, University of Illinois at Urbana–Champaign, Urbana, IL 61801 USA (e-mail: suyan@illinois.edu; kzhang18@illinois.edu; j-jin1@illinois.edu).

Color versions of one or more of the figures in this paper are available online at http://ieeexplore.ieee.org.

Digital Object Identifier 10.1109/TMTT.2017.2785800

0018-9480 © 2018 IEEE. Personal use is permitted, but republication/redistribution requires IEEE permission.
See http://www.ieee.org/publications_standards/publications/rights/index.html for more information.

highly accurate dual-field excitation for the waveports that support the TEM or TE/TM modes, and then present a single-field excitation for general inhomogeneous waveports for which the modal profiles change with the frequency and the modal impedances do not have an explicit dependence on the frequency. With the application of the TF/SF method, the transmitted and reflected waves at the waveports can be obtained easily for the calculation of the S-parameters.

To obtain the modal profiles required in the implementation of the TF/SF method, a novel eigenmode solver is proposed, which calculates directly the transverse electric and magnetic fields ($\mathbf{E}_t$ and $\mathbf{H}_t$) and the propagation constant β. The eigensystem is formulated and solved using the finite-element method (FEM) with edge elements [23] and the calculated modal profiles are then interpolated for the DGTD calculation.

II. DGTD Formulation

To make the formulation easy to understand, we formulate the DGTD equations for the physical region of the device and the PML region separately and then discuss the use of a hybrid mesh in the PML region.

A. DGTD Equations in the Physical Region

Consider Maxwell's equations in the time domain

$$\mu \frac{\partial \mathbf{H}}{\partial t} = -\nabla \times \mathbf{E} \tag{1}$$

$$\varepsilon \frac{\partial \mathbf{E}}{\partial t} = \nabla \times \mathbf{H} - \sigma \mathbf{E} \tag{2}$$

where ε is the permittivity, μ is the permeability, and σ is the conductivity. To obtain a stable DGTD solution for the case with $\sigma > 0$, we employ the leap-frog method to discretize (1) and (2), resulting in the following time-marching equations for each element:

$$H_x^{n+\frac{1}{2}} = H_x^{n-\frac{1}{2}} - \frac{\Delta t}{\mu}\mathbb{M}^{-1}\left[\mathbb{S}_y E_z^n - \mathbb{S}_z E_y^n - \sum_{f=1}^{N_f}\mathbb{M}_f(\hat{n}\times\mathbf{E}^n - \hat{n}\times\mathbf{E}^{n,*})_x\right] \tag{3}$$

$$H_y^{n+\frac{1}{2}} = H_y^{n-\frac{1}{2}} - \frac{\Delta t}{\mu}\mathbb{M}^{-1}\left[\mathbb{S}_z E_x^n - \mathbb{S}_x E_z^n - \sum_{f=1}^{N_f}\mathbb{M}_f(\hat{n}\times\mathbf{E}^n - \hat{n}\times\mathbf{E}^{n,*})_y\right] \tag{4}$$

$$H_z^{n+\frac{1}{2}} = H_z^{n-\frac{1}{2}} - \frac{\Delta t}{\mu}\mathbb{M}^{-1}\left[\mathbb{S}_x E_y^n - \mathbb{S}_y E_x^n - \sum_{f=1}^{N_f}\mathbb{M}_f(\hat{n}\times\mathbf{E}^n - \hat{n}\times\mathbf{E}^{n,*})_z\right] \tag{5}$$

and

$$E_x^{n+1} = \frac{1-\frac{\Delta t\sigma}{2\varepsilon}}{1+\frac{\Delta t\sigma}{2\varepsilon}}E_x^n + \frac{\Delta t}{\varepsilon+\frac{\sigma\Delta t}{2}}\mathbb{M}^{-1} \times\left[\mathbb{S}_y H_z^{n+\frac{1}{2}} - \mathbb{S}_z H_y^{n+\frac{1}{2}} - \sum_{f=1}^{N_f}\mathbb{M}_f \times\left(\hat{n}\times\mathbf{H}^{n+\frac{1}{2}} - \hat{n}\times\mathbf{H}^{n+\frac{1}{2},*}\right)_x\right] \tag{6}$$

$$E_y^{n+1} = \frac{1-\frac{\Delta t\sigma}{2\varepsilon}}{1+\frac{\Delta t\sigma}{2\varepsilon}}E_y^n + \frac{\Delta t}{\varepsilon+\frac{\sigma\Delta t}{2}}\mathbb{M}^{-1} \times\left[\mathbb{S}_z H_x^{n+\frac{1}{2}} - \mathbb{S}_x H_z^{n+\frac{1}{2}} - \sum_{f=1}^{N_f}\mathbb{M}_f \times\left(\hat{n}\times\mathbf{H}^{n+\frac{1}{2}} - \hat{n}\times\mathbf{H}^{n+\frac{1}{2},*}\right)_y\right] \tag{7}$$

$$E_z^{n+1} = \frac{1-\frac{\Delta t\sigma}{2\varepsilon}}{1+\frac{\Delta t\sigma}{2\varepsilon}}E_z^n + \frac{\Delta t}{\varepsilon+\frac{\sigma\Delta t}{2}}\mathbb{M}^{-1} \times\left[\mathbb{S}_x H_y^{n+\frac{1}{2}} - \mathbb{S}_y H_x^{n+\frac{1}{2}} - \sum_{f=1}^{N_f}\mathbb{M}_f \times\left(\hat{n}\times\mathbf{H}^{n+\frac{1}{2}} - \hat{n}\times\mathbf{H}^{n+\frac{1}{2},*}\right)_z\right] \tag{8}$$

where the mass matrices $\mathbb{M}$ and $\mathbb{M}_f$ and the stiffness matrix $\mathbb{S}$ are defined as

$$[\mathbb{M}]_{l,p} = \int_D \varphi_l \varphi_p dv \tag{9}$$

$$[\mathbb{M}_f]_{l,p} = \int_{S_f} \varphi_l \varphi_p ds \tag{10}$$

$$[\mathbb{S}_i]_{l,p} = \int_D \frac{\partial \varphi_l}{\partial i}\varphi_p dv, \quad i \in \{x, y, z\} \tag{11}$$

in which φ_l and φ_p are the Lagrange polynomials in the element domain D bounded by the surface S_f, with $1 \leq (l, p) \leq N$ and N being the total number interpolation points in the element. The numerical fluxes $\hat{n}\times\mathbf{E}^*$ of step n and $\hat{n}\times\mathbf{H}^*$ of step $n+(1/2)$ are defined as

$$\hat{n}\times\mathbf{E}^{n,*} = \hat{n}\times(\mathbf{E}^{n,-}+\mathbf{E}^{n,+}) + \frac{\hat{n}\times\left[\hat{n}\times\left(\mathbf{H}^{n-\frac{1}{2},+}-\mathbf{H}^{n-\frac{1}{2},-}\right)\right]}{Y^+ + Y^-} \tag{12}$$

$$\hat{n}\times\mathbf{H}^{n+\frac{1}{2},*} = \hat{n}\times\left(\mathbf{H}^{n+\frac{1}{2},-}+\mathbf{H}^{n+\frac{1}{2},+}\right) + \frac{\hat{n}\times[\hat{n}\times(\mathbf{E}^{n,+}-\mathbf{E}^{n,-})]}{Z^+ + Z^-} \tag{13}$$

where $\hat{n}$ is the outward normal vector of the element face, and the superscripts "+" and "−" denote the exterior and interior values on the face, respectively. The impedance Z and admittance Y are defined as $Z^\pm = 1/Y^\pm = (\mu^\pm/\varepsilon^\pm)^{1/2}$.

B. DGTD Equations in the PML Region

In the PML region used to truncate the waveports, Maxwell's equations are augmented with two auxiliary-differential equations [24]

$$\mu\frac{\partial \mathbf{H}}{\partial t} = -\nabla\times\mathbf{E} - \mathbf{P} - \mu\bar{\bar{A}}_1\cdot\mathbf{H} \tag{14}$$

$$\frac{\partial \mathbf{P}}{\partial t} = -\bar{\bar{A}}_2\cdot\mathbf{P} + \mu\bar{\bar{A}}_3\cdot\mathbf{H} \tag{15}$$

$$\varepsilon\frac{\partial \mathbf{E}}{\partial t} = \nabla\times\mathbf{H} - \mathbf{Q} - \varepsilon\bar{\bar{A}}_1\cdot\mathbf{E} \tag{16}$$

$$\frac{\partial \mathbf{Q}}{\partial t} = -\bar{\bar{A}}_2\cdot\mathbf{Q} + \varepsilon\bar{\bar{A}}_3\cdot\mathbf{E} \tag{17}$$

where $\bar{\bar{A}}_1$, $\bar{\bar{A}}_2$, and $\bar{\bar{A}}_3$ are diagonal tensors given by

$$\begin{aligned}\bar{\bar{A}}_1 &= \mathrm{diag}[\sigma_z+\sigma_y-\sigma_x, \sigma_x+\sigma_z-\sigma_y, \sigma_y+\sigma_x-\sigma_z]\\ \bar{\bar{A}}_2 &= \mathrm{diag}[\sigma_x, \sigma_y, \sigma_z]\\ \bar{\bar{A}}_3 &= \mathrm{diag}[(\sigma_y-\sigma_x)(\sigma_z-\sigma_x), (\sigma_z-\sigma_y)(\sigma_x-\sigma_y),\\ &\qquad \times(\sigma_x-\sigma_z)(\sigma_y-\sigma_z)].\end{aligned}$$

By applying the DGTD with the leap-frog scheme, we obtain the time-marching equations as

$$\begin{aligned}H_x^{n+\frac{1}{2}} &= \mathbb{A}_{11}^x H_x^{n-\frac{1}{2}} - \frac{\Delta t}{\mu}\mathbb{A}_{12}^x\\ &\quad\times\left[\mathbb{S}_y E_z^n - \mathbb{S}_z E_y^n - \sum_{f=1}^{N_f}\mathbb{M}_f\right.\\ &\qquad\left.\times(\hat{n}\times\mathbf{E}^n - \hat{n}\times\mathbf{E}^{n,*})_x\right] - \frac{\Delta t}{\mu}\mathbb{M}P_x^n\end{aligned} \tag{18}$$

$$\begin{aligned}H_y^{n+\frac{1}{2}} &= \mathbb{A}_{11}^y H_y^{n-\frac{1}{2}} - \frac{\Delta t}{\mu}\mathbb{A}_{12}^y\\ &\quad\times\left[\mathbb{S}_z E_x^n - \mathbb{S}_x E_z^n - \sum_{f=1}^{N_f}\mathbb{M}_f\right.\\ &\qquad\left.\times(\hat{n}\times\mathbf{E}^n - \hat{n}\times\mathbf{E}^{n,*})_y\right] - \frac{\Delta t}{\mu}\mathbb{M}P_y^n\end{aligned} \tag{19}$$

$$\begin{aligned}H_z^{n+\frac{1}{2}} &= \mathbb{A}_{11}^z H_y^{n-\frac{1}{2}} - \frac{\Delta t}{\mu}\mathbb{A}_{12}^z\\ &\quad\times\left[\mathbb{S}_x E_y^n - \mathbb{S}_y E_x^n - \sum_{f=1}^{N_f}\mathbb{M}_f\right.\\ &\qquad\left.\times(\hat{n}\times\mathbf{E}^n - \hat{n}\times\mathbf{E}^{n,*})_z\right] - \frac{\Delta t}{\mu}\mathbb{M}P_z^n\end{aligned} \tag{20}$$

where

$$P_x^n = \mathbb{A}_2^x\ P_x^{n-1} + \mu\mathbb{A}_3^x\ H_x^{n-\frac{1}{2}} \tag{21}$$

$$P_y^n = \mathbb{A}_2^y\ P_y^{n-1} + \mu\mathbb{A}_3^y H_y^{n-\frac{1}{2}} \tag{22}$$

$$P_z^n = \mathbb{A}_2^z\ P_z^{n-1} + \mu\mathbb{A}_3^z H_z^{n-\frac{1}{2}} \tag{23}$$

and

$$\begin{aligned}E_x^{n+1} &= \mathbb{A}_{11}^x E_x^n + \frac{\Delta t}{\varepsilon}\mathbb{A}_{12}^x\\ &\quad\times\left[\mathbb{S}_y H_z^{n+\frac{1}{2}} - \mathbb{S}_z H_y^{n+\frac{1}{2}} - \sum_{f=1}^{N_f}\mathbb{M}_f\right.\\ &\qquad\left.\times\left(\hat{n}\times\mathbf{H}^{n+\frac{1}{2}} - \hat{n}\times\mathbf{H}^{n+\frac{1}{2},*}\right)_x\right] - \frac{\Delta t}{\mu}\mathbb{M}Q_x^{n+\frac{1}{2}}\end{aligned} \tag{24}$$

$$\begin{aligned}E_y^{n+1} &= \mathbb{A}_{11}^y E_y^n + \frac{\Delta t}{\varepsilon}\mathbb{A}_{12}^y\\ &\quad\times\left[\mathbb{S}_z H_x^n - \mathbb{S}_x H_z^n - \sum_{f=1}^{N_f}\mathbb{M}_f\right.\\ &\qquad\left.\times\left(\hat{n}\times\mathbf{H}^{n+\frac{1}{2}} - \hat{n}\times\mathbf{H}^{n+\frac{1}{2},*}\right)_y\right] - \frac{\Delta t}{\mu}\mathbb{M}Q_y^{n+\frac{1}{2}}\end{aligned} \tag{25}$$

$$\begin{aligned}E_z^{n+1} &= \mathbb{A}_{11}^z E_y^n + \frac{\Delta t}{\varepsilon}\mathbb{A}_{12}^z\\ &\quad\times\left[\mathbb{S}_x H_y^{n+\frac{1}{2}} - \mathbb{S}_y H_x^{n+\frac{1}{2}} - \sum_{f=1}^{N_f}\mathbb{M}_f\right.\\ &\qquad\left.\times\left(\hat{n}\times\mathbf{H}^{n+\frac{1}{2}} - \hat{n}\times\mathbf{H}^{n+\frac{1}{2},*}\right)_z\right] - \frac{\Delta t}{\mu}\mathbb{M}Q_z^{n+\frac{1}{2}}\end{aligned} \tag{26}$$

where

$$Q_x^{n+\frac{1}{2}} = \mathbb{A}_2^x\ Q_x^{n-\frac{1}{2}} + \varepsilon\mathbb{A}_3^x\ E_x^n \tag{27}$$

$$Q_y^{n+\frac{1}{2}} = \mathbb{A}_2^y\ Q_y^{n-\frac{1}{2}} + \varepsilon\mathbb{A}_3^y E_y^n \tag{28}$$

$$Q_z^{n+\frac{1}{2}} = \mathbb{A}_2^z\ Q_z^{n-\frac{1}{2}} + \varepsilon\mathbb{A}_3^z E_z^n. \tag{29}$$

In (27)–(29)

$$\mathbb{A}_{11}^i = \left(\mathbb{M} + \frac{\Delta t}{2}\mathbb{M}_{\bar{\bar{A}}_1}^i\right)^{-1}\left(\mathbb{M} - \frac{\Delta t}{2}\mathbb{M}_{\bar{\bar{A}}_1}^i\right) \tag{30}$$

$$\mathbb{A}_{12}^i = \left(\mathbb{M} + \frac{\Delta t}{2}\mathbb{M}_{\bar{\bar{A}}_1}^i\right)^{-1} \tag{31}$$

$$\mathbb{A}_2^i = \left(\mathbb{M} + \frac{\Delta t}{2}\mathbb{M}_{\bar{\bar{A}}_2}^i\right)^{-1}\left(\mathbb{M} - \frac{\Delta t}{2}\mathbb{M}_{\bar{\bar{A}}_2}^i\right) \tag{32}$$

$$\mathbb{A}_3^i = \left(\mathbb{M} + \frac{\Delta t}{2}\mathbb{M}_{\bar{\bar{A}}_3}^i\right)^{-1}\left(\Delta t\mathbb{M}_{\bar{\bar{A}}_3}^i\right) \tag{33}$$

where $i \in \{x, y, z\}$ and the involved mass matrices are defined as

$$\left[\mathbb{M}_{\bar{\bar{A}}_1}^x\right]_{l,p} = \int_D (\sigma_z+\sigma_y-\sigma_x)\varphi_l\varphi_p dv \tag{34}$$

$$\left[\mathbb{M}_{\bar{\bar{A}}_1}^y\right]_{l,p} = \int_D (\sigma_x+\sigma_z-\sigma_y)\varphi_l\varphi_p dv \tag{35}$$

$$\left[\mathbb{M}_{\bar{\bar{A}}_1}^z\right]_{l,p} = \int_D (\sigma_y+\sigma_x-\sigma_z)\varphi_l\varphi_p dv \tag{36}$$

$$\left[\mathbb{M}_{A_2}^i\right]_{l,p} = \int_D \sigma_i\varphi_l\varphi_p dv, \quad i \in \{x, y, z\} \tag{37}$$

$$[\mathbb{M}^x_{\bar{\bar{A}}_3}]_{l,p} = \int_D (\sigma_y - \sigma_x)(\sigma_z - \sigma_x)\varphi_l \varphi_p dv \tag{38}$$

$$[\mathbb{M}^y_{\bar{\bar{A}}_3}]_{l,p} = \int_D (\sigma_z - \sigma_y)(\sigma_x - \sigma_y)\varphi_l \varphi_p dv \tag{39}$$

$$[\mathbb{M}^z_{\bar{\bar{A}}_3}]_{l,p} = \int_D (\sigma_x - \sigma_z)(\sigma_y - \sigma_z)\varphi_l \varphi_p dv. \tag{40}$$

As in the FDTD implementation, the conductivity parameters have a gradual increase in the PML region as $\sigma_i = \sigma^i_{\max}(d^i/d^i_{\max})^v$ $(i \in \{x, y, z\})$, where d^i denotes the distance from the PML surface and $d^i_{\max}$ is the thickness of the PML. The value of $\sigma^i_{\max}$ is calculated as [24]

$$\sigma^i_{\max} = \frac{0.8(v+1)}{\Delta d\sqrt{\varepsilon_{\mathrm{m}}\mu_{\mathrm{m}}}} \tag{41}$$

where Δd is the cell size in the PML region, ε_{m} and μ_{m} are the mean values of the relative permittivity and permeability, respectively, and v is usually chosen to be 2 or 3 for an optimal performance.

C. Hybrid Mesh in the PML Region

To facilitate the use of the PML in engineering applications, the mesh in the PML region can be extruded automatically from the mesh in the physical region of the device. With such an extrusion, the elements in the PML region will take the form of either a hexahedron or a wedge (triangular prism), depending on the types of the elements used in the physical region (see Fig. 1). More importantly, since the mass matrices of hexahedral and wedge elements can be made diagonal or block diagonal by choosing appropriate interpolation and quadrature points, the computational efficiency in the PML region can be enhanced significantly and the associated memory usage can be reduced. Such cannot be done, however, with a tetrahedral mesh because for tetrahedral elements, the mass matrices are not diagonal and since the values of σ_x, σ_y, and σ_z vary within each element, the associated coefficient matrices $\mathbb{A}^i_{11}$, $\mathbb{A}^i_{12}$, $\mathbb{A}^i_2$, and $\mathbb{A}^i_3$ cannot be calculated by scaling the matrices of a reference element.

For hexahedral elements, the basis functions proposed in [25] are used in this paper. By letting $\vec{\xi} = (\xi_m, \xi_n, \xi_q)$ with $1 \le (m, n, q) \le r+1$ being a set of points, r being the order of the basis functions, and ξ_l being the Gaussian points defined in [0, 1], the tensorial basis functions are defined as

$$\varphi_{m,n,q} = \phi_m(x)\phi_n(y)\phi_q(z) \tag{42}$$

where ϕ_m denote the Lagrange interpolation polynomials

$$\phi_m(x) = \frac{\Pi_{s\neq m}(x - \xi_s)}{\Pi_{s\neq m}(\xi_m - \xi_s)}. \tag{43}$$

Using the Gauss quadrature method, we obtain a diagonal mass matrix

$$\mathbb{M} = \mathrm{diag}[w_1, w_2, ..., w_N] \tag{44}$$

where w_l with $l \in \{1, 2, ..., N\}$ is the Gauss quadrature weight of the lth point and $N = 3(r+1)$ is the total number of interpolation points in a hexahedral element. Consequently, the matrices $\mathbb{M}^i_{A_1}$, $\mathbb{M}^i_{A_2}$, and $\mathbb{M}^i_{A_3}$ with $i \in \{x, y, z\}$ are also diagonal, which can be obtained easily by multiplying the mass matrices for a reference element with corresponding transformation coefficients.

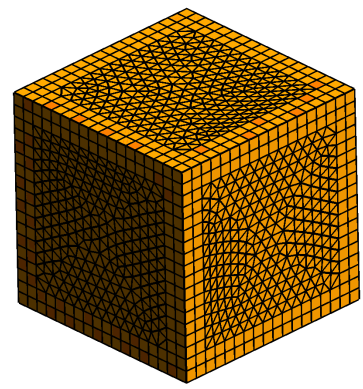

Fig. 1. Hybrid mesh with hexahedral and wedge elements used for the overlapping and nonoverlapping PML regions.

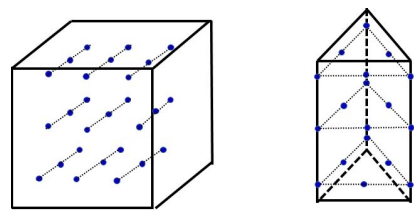

Fig. 2. Interpolation points on a second-order hexahedral and wedge element.

For wedge elements, a block-diagonal mass matrix can be obtained by using the Gaussian points for the longitudinal direction and the Gauss–Lobatto points for the transverse plane, as shown in Fig. 2. The basis functions for a wedge element are obtained by a tensor product between the nodal functions of a triangular element (ϕ^{T}_p) and the Lagrange interpolation functions (ϕ^{L}_k) as

$$\varphi_{pk} = \phi^{\mathrm{T}}_p \phi^{\mathrm{L}}_k. \tag{45}$$

As a result, the mass matrix can be calculated as

$$\mathbb{M} = M_{\mathrm{L}} \otimes M_{\mathrm{T}} \tag{46}$$

where

$$M_{\mathrm{L}} = \int_c [\phi^{\mathrm{L}}_k \phi^{\mathrm{L}}_m] dl \qquad M_{\mathrm{T}} = \int_s [\phi^{\mathrm{T}}_p \phi^{\mathrm{T}}_q] ds \tag{47}$$

in which c denotes the length of the wedge element and s denotes the triangular cross section of the element. As M_{L} is a diagonal matrix and M_{T} is a dense matrix, $\mathbb{M}$ is a block-diagonal matrix, and so are the matrices $\mathbb{M}^i_{A_1}$, $\mathbb{M}^i_{A_2}$, and $\mathbb{M}^i_{A_3}$. Consequently, we obtain

$$\mathbb{A}^i_{11} = A^i_{11,L} \otimes I_{\mathrm{T}} \tag{48}$$

$$\mathbb{A}^i_{12} = A^i_{12,L} \otimes M^{-1}_{\mathrm{T}} \tag{49}$$

$$\mathbb{A}^i_2 = A^i_{2,L} \otimes I_{\mathrm{T}} \tag{50}$$

$$\mathbb{A}^i_3 = A^i_{3,L} \otimes I_{\mathrm{T}} \tag{51}$$

where $i \in \{x, y, z\}$, $\mathbb{A}^i_{11,L}$, $\mathbb{A}^i_{12,L}$, $\mathbb{A}^i_{2,L}$, and $\mathbb{A}^i_{3,L}$ are the corresponding longitudinal matrices, and I_{T} is a unit matrix with the same dimension as M_{T}.

From the formulation above, it can be observed that one needs to store only $\mathbb{A}_{11}^i$, $\mathbb{A}_{12}^i$, $\mathbb{A}_2^i$, and $\mathbb{A}_3^i$ for hexahedral elements and $\mathbb{A}_{11,L}^i$, $\mathbb{A}_{12,L}^i$ $\mathbb{A}_{2,L}^i$, and $\mathbb{A}_{3,L}^i$ for wedge elements, and because all these matrices are diagonal, the overall memory usage and computational cost for the calculation in the PML region can be reduced significantly.

III. Modal Solver

For a general waveport whose modal functions cannot be derived analytically, the FEM can be used to compute the modal profiles and the propagation constants in the frequency domain. Consider the source-free curl–curl equations for $\mathbf{E}$ and $\mathbf{H}$

$$\nabla \times \left(\frac{1}{\mu}\nabla \times \mathbf{E}\right) - \omega^2 \varepsilon \mathbf{E} = 0 \tag{52}$$

$$\nabla \times \left(\frac{1}{\varepsilon}\nabla \times \mathbf{H}\right) - \omega^2 \mu \mathbf{H} = 0. \tag{53}$$

In a waveguiding system, the electric and magnetic fields are assumed to have the form

$$\mathbf{E} = [\mathbf{E}_{\mathrm{t}}(x, y) + E_z(x, y)\hat{z}]e^{-j\beta z} \tag{54}$$

$$\mathbf{H} = [\mathbf{H}_{\mathrm{t}}(x, y) + H_z(x, y)\hat{z}]e^{-j\beta z}. \tag{55}$$

The gradient operator can then be decomposed as

$$\nabla = \hat{x}\partial_x + \hat{y}\partial_y + \hat{z}\partial_z = \nabla_{\mathrm{t}} - j\beta\hat{z}. \tag{56}$$

With these, one can obtain

$$\nabla_{\mathrm{t}} \times \left(\frac{1}{\mu}\nabla_{\mathrm{t}} \times \mathbf{E}_{\mathrm{t}}\right) - \omega^2 \varepsilon \mathbf{E}_{\mathrm{t}} = \frac{\beta}{\mu}(j\nabla_{\mathrm{t}} E_z - \beta \mathbf{E}_{\mathrm{t}}) \tag{57}$$

$$\nabla_{\mathrm{t}} \times \left(\frac{1}{\varepsilon}\nabla_{\mathrm{t}} \times \mathbf{H}_{\mathrm{t}}\right) - \omega^2 \mu \mathbf{H}_{\mathrm{t}} = \frac{\beta}{\varepsilon}(j\nabla_{\mathrm{t}} H_z - \beta \mathbf{H}_{\mathrm{t}}). \tag{58}$$

By taking the transverse components of Maxwell's equations, we obtain

$$j\nabla_{\mathrm{t}} E_z - \beta \mathbf{E}_{\mathrm{t}} = \omega\mu\hat{z} \times \mathbf{H}_{\mathrm{t}} \tag{59}$$

$$j\nabla_{\mathrm{t}} H_z - \beta \mathbf{H}_{\mathrm{t}} = -\omega\varepsilon\hat{z} \times \mathbf{E}_{\mathrm{t}}. \tag{60}$$

Substituting these two equations into (57) and (58) yields the two equations for the transverse fields as

$$\nabla_{\mathrm{t}} \times \left(\frac{1}{\mu}\nabla_{\mathrm{t}} \times \mathbf{E}_{\mathrm{t}}\right) - \omega^2 \varepsilon \mathbf{E}_{\mathrm{t}} = \beta\omega\hat{z} \times \mathbf{H}_{\mathrm{t}} \tag{61}$$

$$\nabla_{\mathrm{t}} \times \left(\frac{1}{\varepsilon}\nabla_{\mathrm{t}} \times \mathbf{H}_{\mathrm{t}}\right) - \omega^2 \mu \mathbf{H}_{\mathrm{t}} = -\beta\omega\hat{z} \times \mathbf{E}_{\mathrm{t}}. \tag{62}$$

By applying the FEM with edge basis functions to these two equations [23], we can obtain a generalized eigensystem

$$Ab = \lambda M b \tag{63}$$

where $\lambda = \beta$ and $b = [E_{\mathrm{t}}, H_{\mathrm{t}}]^{\mathrm{T}}$. The mesh to be used for the FEM discretization can be extracted from the 3-D mesh of the physical device. The ARPACK package can be used to solve this eigensystem [26]. The solution yields the propagation constants β_n and the transverse components of the modal functions $\mathbf{e}_n$ and $\mathbf{h}_n$, with n being the modal index and $\mathbf{e}_n$ and $\mathbf{h}_n$ normalized as

$$\int_{S_{\mathrm{p}}} (\mathbf{e}_n \times \mathbf{h}_n) \cdot d\mathbf{s} = 1 \tag{64}$$

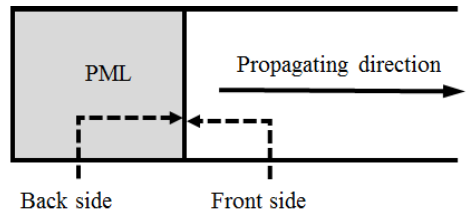

Fig. 3. PML-terminated waveport with the excitation surface coinciding with the PML surface.

where S_{p} denotes the cross section of the waveport. Different from the traditional modal solvers that calculate β^2 as the eigenvalues and either $\mathbf{E}$ or $\mathbf{H}$ as the eigenvectors, this modal solver calculates directly β and both $\mathbf{E}_{\mathrm{t}}$ and $\mathbf{H}_{\mathrm{t}}$, which can be directly adopted for the proposed waveport excitation and S-parameter extraction.

IV. Excitation and S-Parameter Extraction

To excite a waveport and extract S-parameters, two numerical schemes are formulated in this paper based on the TF/SF method. The excitation is assigned on the surface between the PML region and the physical region, as shown in Fig. 3. For waveports that support the TEM or TE/TM modes, a dual-field excitation scheme can be formulated such that it excites only the incident wave toward the device and no waves toward the PML. Therefore, the SF can be obtained directly from the field on the back side of the excitation surface. This unidirectional excitation can yield a more accurate S-parameter calculation. For general waveports such as inhomogeneous waveports with an unknown frequency dependence of the modal impedance, the excitation can only be introduced through a single field, which excites the incident wave on both directions. In such a case, the SF is obtained by subtracting the incident field from the TF on the front side of the excitation surface. Fortunately, the accuracy of the single-field-based scheme can be improved simply by using more PML layers.

A. TEM Excitation

For the TEM mode, the wave impedance is a constant given by $Z = (\mu/\varepsilon)^{1/2}$ and the propagation constant is given by $\beta = \omega(\varepsilon\mu)^{1/2}$. Since both the incident fields $\mathbf{E}^{\mathrm{inc}}$ and $\mathbf{H}^{\mathrm{inc}}$ are known, the excitation can be effected in the DGTD equations by modifying the numerical fluxes at the excitation surface as

$$\hat{n} \times \mathbf{E}^* = \hat{n} \times (\mathbf{E}^- + \mathbf{E}^+ + \mathbf{E}^{\mathrm{inc}}) + \frac{\hat{n} \times [\hat{n} \times (\mathbf{H}^+ - \mathbf{H}^- + \mathbf{H}^{\mathrm{inc}})]}{Y^+ + Y^-} \tag{65}$$

$$\hat{n} \times \mathbf{H}^* = \hat{n} \times (\mathbf{H}^- + \mathbf{H}^+ + \mathbf{H}^{\mathrm{inc}}) + \frac{\hat{n} \times [\hat{n} \times (\mathbf{E}^+ - \mathbf{E}^- + \mathbf{E}^{\mathrm{inc}})]}{Y^+ + Y^-} \tag{66}$$

where $\mathbf{E}^{\mathrm{inc}} = \mathbf{e}_n g(t)$ and $\mathbf{H}^{\mathrm{inc}} = \mathbf{h}_n g(t)$ for the numerical fluxes at the front side, and $\mathbf{E}^{\mathrm{inc}} = -\mathbf{e}_n g(t)$ and $\mathbf{H}^{\mathrm{inc}} = -\mathbf{h}_n g(t)$ for the numerical fluxes on the back side of the excitation surface. Here, $(\mathbf{e}_n, \mathbf{h}_n)$ represents the modal function of the TEM mode to be excited and $g(t)$ is the temporal profile of the input signal, which can be a Gaussian or a modulated

Gaussian pulse. This is equivalent to using an electric current sheet $\mathbf{J}_s = \hat{n} \times \mathbf{H}^{inc}$ and a magnetic current sheet $\mathbf{M}_s = \mathbf{E}^{inc} \times \hat{n}$ to excite the waveport. When the fields excited by the two current sheets are combined, it will produce $(\mathbf{E}^{inc}, \mathbf{H}^{inc})$ in the forward direction and a null field in the backward direction.

B. TE/TM Excitation

For the TE/TM modes, the mode profiles are frequency-independent and the wave impedances change with the frequency in a known explicit form. Hence, both the incident fields $\mathbf{E}^{inc}$ and $\mathbf{H}^{inc}$ can be obtained and the excitation can be effected in the DGTD equations in the same manner as for the TEM mode. For example, for the TE modes, we have [27]

$$\mathbf{H}_t = -\frac{j\beta}{k_c^2}\nabla_t H_z \tag{67}$$

$$\mathbf{E}_t = \frac{j\omega}{c}\left(\frac{\eta}{k_c^2}\hat{z} \times \nabla_t H_z\right) \tag{68}$$

where k_c is the cutoff wavenumber and c is the speed of light. Defining $s = j\omega$, we have

$$\mathbf{H}_t = \sqrt{\frac{s^2}{c^2} + k_c^2}\left(\frac{1}{k_c^2}\nabla_t H_z\right) \tag{69}$$

$$\mathbf{E}_t = \frac{s}{c}\left(\frac{\eta}{k_c^2}\hat{z} \times \nabla_t H_z\right). \tag{70}$$

Since H_z is frequency-independent, we only need to apply the inverse Laplace transform to $(s^2/c^2 + k^2)^{1/2}$ and s/c in (69) and (70) to obtain

$$L^{-1}\left\{\frac{s}{c}\right\} = \frac{d}{dt} \tag{71}$$

$$L^{-1}\left\{\sqrt{\frac{s^2}{c^2} + k_c^2}\right\} = \frac{d}{dt} + \frac{k_c}{t}J_1(k_c ct)u(t)* \tag{72}$$

where J_1 denotes the first-order Bessel function, $u(t)$ denotes the unit step function, and $*$ denotes time convolution. With these, the incident fields for the TE modes can be formulated as

$$\mathbf{E}^{inc} = \frac{dg(t)}{dt}\mathbf{e}_n \tag{73}$$

$$\mathbf{H}^{inc} = \left[\frac{dg(t)}{dt} + \frac{k_c}{t}J_1(k_c ct)u(t) * g(t)\right]\mathbf{h}_n. \tag{74}$$

The incident fields for the TM modes can be formulated similarly as

$$\mathbf{E}^{inc} = \left[\frac{dg(t)}{dt} + \frac{k_c}{t}J_1(k_c ct)u(t) * g(t)\right]\mathbf{e}_n \tag{75}$$

$$\mathbf{H}^{inc} = \frac{dg(t)}{dt}\mathbf{h}_n. \tag{76}$$

C. Excitation at an Inhomogeneous Waveport

For an inhomogeneous waveport, the modal profiles change with the frequency and the wave impedances also change with the frequency. Since the dependence of the wave impedances on the frequency is not known analytically, one cannot obtain both the incident electric and magnetic fields at all the frequencies of interest. One approach to alleviating this problem is to use the modal solver to compute the wave impedance of the mode to be excited over the frequency range of interest and derive an analytical approximation so that both $\mathbf{E}^{inc}$ and $\mathbf{H}^{inc}$ can be used to excite the mode. This approach is too cumbersome for practical application. A simpler alternative is to excite the waveport using only one field, either $\mathbf{E}^{inc}$ or $\mathbf{H}^{inc}$, computed at the central frequency. For example, if we choose to use $\mathbf{E}^{inc}$ to excite the waveport, we set the numerical fluxes at the front side of the excitation surface as

$$\begin{aligned}\hat{n} \times \mathbf{E}^* &= \hat{n} \times (\mathbf{E}^- + \mathbf{E}^+ + 2\mathbf{E}^{inc}) \\ &\quad + \frac{\hat{n} \times [\hat{n} \times (\mathbf{H}^+ - \mathbf{H}^-)]}{Y^+ + Y^-}\end{aligned} \tag{77}$$

$$\begin{aligned}\hat{n} \times \mathbf{H}^* &= \hat{n} \times (\mathbf{H}^- + \mathbf{H}^+) \\ &\quad + \frac{\hat{n} \times [\hat{n} \times (\mathbf{E}^+ - \mathbf{E}^- + 2\mathbf{E}^{inc})]}{Z^+ + Z^-}\end{aligned} \tag{78}$$

and the numerical fluxes at the back side as

$$\begin{aligned}\hat{n} \times \mathbf{E}^* &= \hat{n} \times (\mathbf{E}^- + \mathbf{E}^+ - 2\mathbf{E}^{inc}) \\ &\quad + \frac{\hat{n} \times [\hat{n} \times (\mathbf{H}^+ - \mathbf{H}^-)]}{Y^+ + Y^-}\end{aligned} \tag{79}$$

$$\begin{aligned}\hat{n} \times \mathbf{H}^* &= \hat{n} \times (\mathbf{H}^- + \mathbf{H}^+) \\ &\quad + \frac{\hat{n} \times [\hat{n} \times (\mathbf{E}^+ - \mathbf{E}^- - 2\mathbf{E}^{inc})]}{Z^+ + Z^-}.\end{aligned} \tag{80}$$

This is equivalent to using a magnetic current sheet $\mathbf{M}_s = 2\mathbf{E}^{inc} \times \hat{n}$ to excite the waveport, which will produce $(\mathbf{E}^{inc}, \mathbf{H}^{inc})$ on both sides of the excitation surface. Even though the modal profiles of an inhomogeneous waveport vary with the frequency, the change for the dominant mode is usually not drastic and the results obtained with the modal profile at the central frequency are found to be sufficiently accurate [9]. Since the single-field excitation scheme excites the waves on the both sides of the excitation surface, including evanescent waves, the PML can have a larger effect on the calculation of the reflected field and hence the S-parameters. This problem can, however, be alleviated by increasing the number of the PML layers to improve its absorption performance.

D. S-Parameter Extraction

Once the fields at the waveports are computed, the S-parameters of a multiport device can be calculated as

$$S_{(i,n),(j,m)} = \frac{F\{b_{i,n}\}}{F\{a_{j,m}\}} \tag{81}$$

where F denotes the Fourier transform, $a_{j,m}$ denotes the modal coefficient of the excitation of mode m at port j, and $b_{i,n}$ denotes the modal coefficient of the reflected or transmitted waves of mode n at port i. The $a_{j,m}$ can be calculated as

$$a_{j,m} = \int_{S_p} \mathbf{E}_j^{inc} \times \mathbf{h}_m \cdot d\mathbf{s}. \tag{82}$$

The $b_{i,n}$ at a passive port can be calculated similarly as

$$b_{i,n} = \int_{S_p} \mathbf{E}_i \times \mathbf{h}_n \cdot d\mathbf{s}. \tag{83}$$

However, the calculation of $b_{i,n}$ at an active port depends on the use of the excitation scheme.

Since the dual-field excitation scheme excites the incident wave only in the front side of the excitation surface and no waves in the back side of the excitation surface, we can obtain the reflected field directly from the field calculated at the back side and use it as $\mathbf{E}_i$ in the calculation based on (83). For the single-field excitation scheme, the incident wave is excited at both sides of the excitation surface. Therefore, the reflected field has to be calculated by subtracting the incident field from the TF at the front side of the excitation surface as

$$b_{i,n} = \int_{S_\mathrm{p}} \mathbf{E}_i \times \mathbf{h}_n \cdot d\mathbf{s} - a_{i,n}. \tag{84}$$

In the evaluation of the S-parameters described above, we again assumed that for an inhomogeneous waveport, the modal profiles do not change drastically from that of the central frequency. A potential improvement is to compute the modal profile at each frequency of interest using the FEM and use it to calculate the S-parameters. Since the dimension of the eigensystem at the waveports is very small, the computation of the modal profiles is very fast, rendering this improved S-parameter extraction practical for engineering applications.

V. Numerical Results

In this section, a variety of examples are investigated to demonstrate the accuracy of the proposed TF/SF-based scheme for the waveport excitation and S-parameter extraction. All the examples are simulated on a laptop of an Intel Core i7-4900 MQ at 2.8-GHz CPU equipped with 24 GB memory and Linux 64 bit system.

A. Monopole Antenna

The first example is to validate the excitation and S-parameter extraction at a TEM waveport by considering a monopole antenna, similar to the one simulated in [28]. The antenna consists of a conducting cylinder with a 180 mm height and a 3.75 mm diameter placed on a ground plane. A 30-mm-long coaxial line with a 3.75-mm inner radius and 12-mm outer radius is used to feed the antenna. Two layers of PML are used to truncate the open space, as shown in Fig. 4, which includes 19 209 tetrahedra, 208 hexahedra, and 784 prisms. The Gaussian pulse is applied to excite the port, and the input and output signals at the port are shown in Fig. 5. The calculated return loss is given in Fig. 6, which shows good agreement with the results obtained from the frequency-domain FEM solver in ANSYS HFSS.

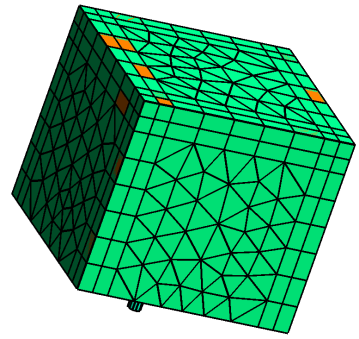

Fig. 4. Mesh configuration of the monopole antenna simulation.

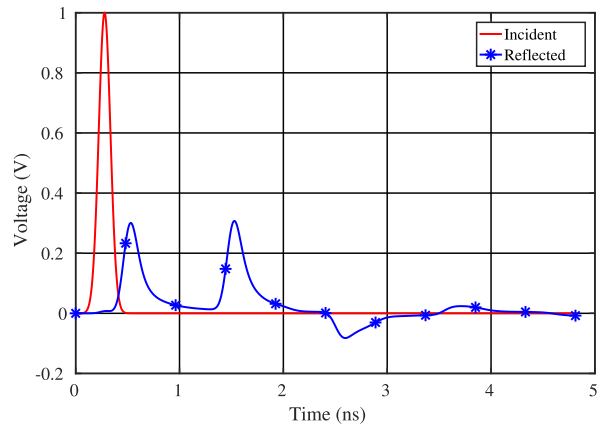

Fig. 5. Incident and reflected voltages at the port of the monopole antenna.

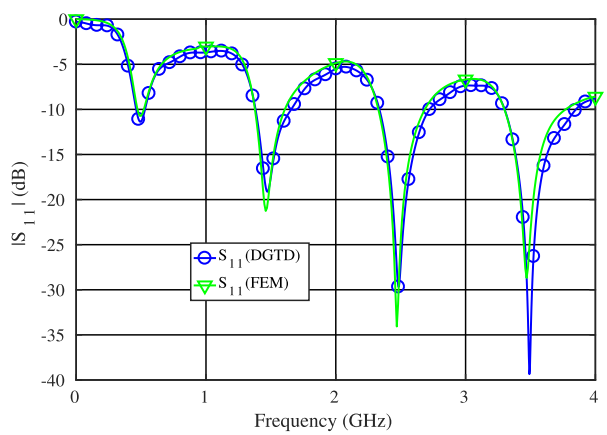

Fig. 6. $|S_{11}|$ of the monopole antenna.

B. Rectangular Waveguide

The second example is to validate the excitation and S-parameter extraction for the TE/TM modes using the dual-field and single-field excitation schemes and compare the performance of these two schemes. The results computed by the frequency-domain FEM are used as the reference. The device to be simulated is a section of an empty waveguide made of the standard WR15 rectangular waveguide with a length of 38.1 mm, a width of 19.5 mm, and a height of 9.525 mm. The TE10 mode is launched at the waveport on the left-hand side. The mesh configuration of the waveguide is shown in Fig. 7, where the physical region is discretized into 1035 tetrahedral elements with third-order basis functions, and the PML regions are discretized into wedge elements.

The S_{11} and S_{21} are calculated by the two schemes with several different configurations. The results are shown in Fig. 8, which shows an excellent accuracy of the dual-field excitation scheme even with only four layers of PML. The accuracy of the single-field excitation scheme is also excellent for the S_{21} calculation, but is relatively poor for the S_{11} calculation

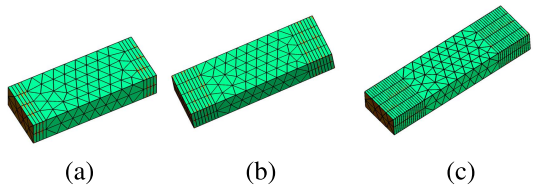

Fig. 7. Meshes of the rectangular waveguide. (a) With four PML layers. (b) With eight PML layers. (c) With 16 PML layers.

below the cutoff, because the single-field scheme excites the fields in both directions and the PML's nonphysical reflection can compromise the calculation of the reflected wave at the excited port. However, this error can be reduced very effectively by increasing the number of PML layers. As can be observed in Fig. 8(a), with eight layers of PML, the error is reduced to the same level as that of the dual-field excitation using four layers of PML. A frequency-domain FEM gives better results because of the usage of WPBC. Further increasing the PML to 16 layers, the accuracy will continue to be improved. However, the level of the improvement is not obvious, even we increase the order of basis function, so we think that PML limits the accuracy. Since usually −40 dB is sufficient for practical application, using eight layers of PML is enough.

C. Inhomogeneous Waveguide

The third example is to validate the waveport excitation and S-parameter extraction at inhomogeneous waveports using the single-field excitation scheme. The geometry to be considered is shown in Fig. 9, which is a rectangular waveguide loaded with two infinitely long dielectric slabs with a relative permittivity of 4 and 2, respectively. Although this is a relatively simple inhomogeneous waveguide, it is quite difficult to simulate and obtain correct results with most commercial softwares based on the time-domain simulation. For this simulation, the first mode calculated at 35 GHz is used to excite the waveport, and eight PML layers are employed to truncate the waveports. The S-parameters S_{11} and S_{21} are computed and displayed in Fig. 10. It can be seen that the calculated S_{11} is below −40 dB from 6 to 50 GHz, and this accuracy is comparable to that of the single-field excitation with eight PML layers for a homogeneous waveguide shown in Fig. 8. Note that the reference solution obtained using the frequency-domain FEM has a better accuracy, because it uses the WBPC at each frequency point.

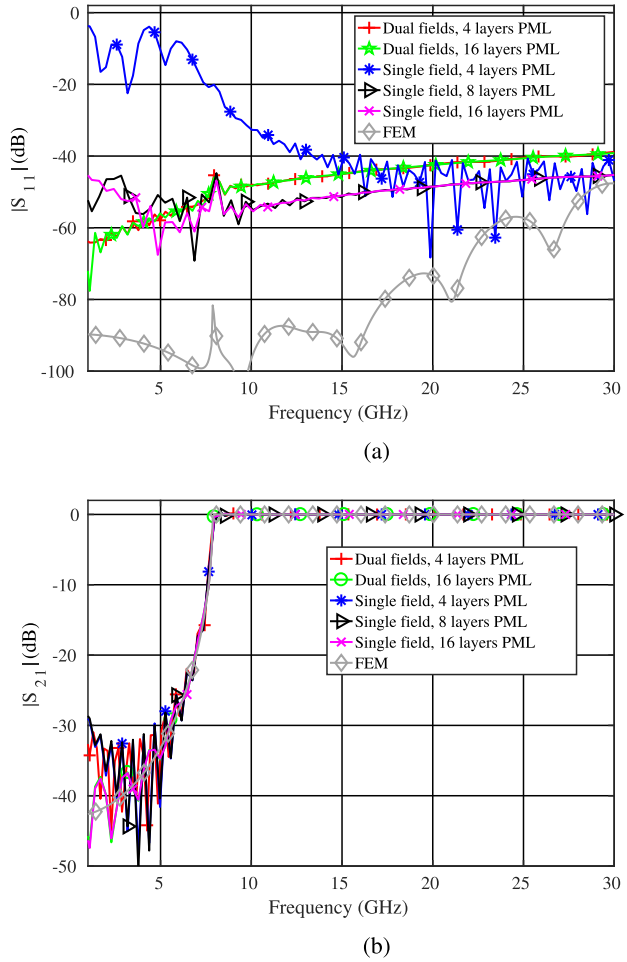

Fig. 8. S-parameters of rectangular waveguide excited with the TE10 mode. (a) $|S_{11}|$. (b) $|S_{21}|$.

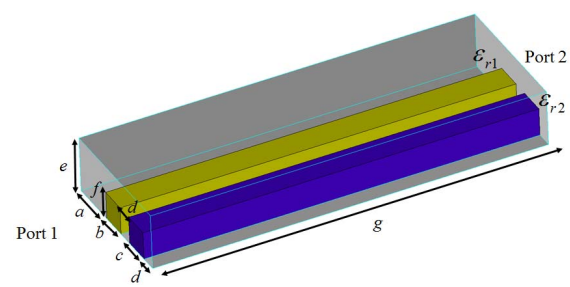

Fig. 9. Geometry of the inhomogeneous waveguide. The dimensions are $a = 1.8$, $b = 1$, $c = 1$, $d = 0.6$, $e = 2$, $f = 1$, and $g = 14$, all in mm; the relative permittivity of the central slab is 4 and that of the side slab is 2.

D. Dielectric-Loaded Waveguide Filter

The next three examples are computed using the single-field excitation as all these examples contain inhomogeneous waveports, the focus of this paper. First, we consider a rectangular waveguide filter, whose geometry is shown in Fig. 11. Such filters have been widely used in a variety of microwave systems and extensively investigated in the literature [29], [30]. It has also been used to serve as a testing case in [9] and [31] to validate the S-parameter extraction for inhomogeneous waveguides. The waveguide filter contains four dielectric blocks that are centered in the transverse direction and extend over the full height of the waveguide. The filter is symmetric with respect to the longitudinal center, and all the blocks have the same width of $b = 1$ mm. At the input port (port 1) and the output port (port 2), the dielectric blocks have a relative permittivity of $\epsilon_{r1} = 9.7$ and the distance to the next dielectric block is $e = 2$ mm. The two blocks located in the middle of the filter have a length of $f = 2$ mm and a relative permittivity of $\epsilon_{r2} = 7.0$. The distance between these two dielectric blocks is $g = 4$ mm.

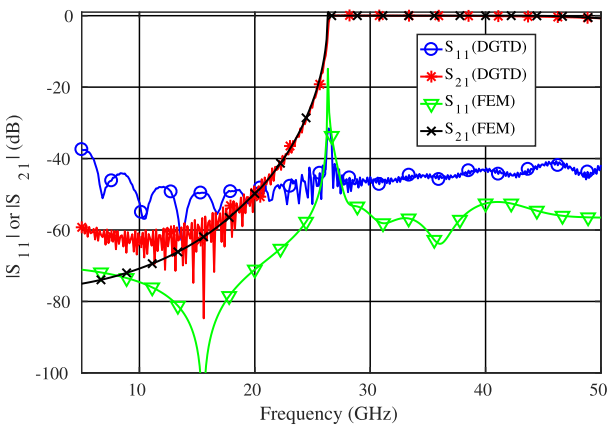

Fig. 10. $|S_{11}|$ and $|S_{21}|$ of the inhomogeneous waveguide.

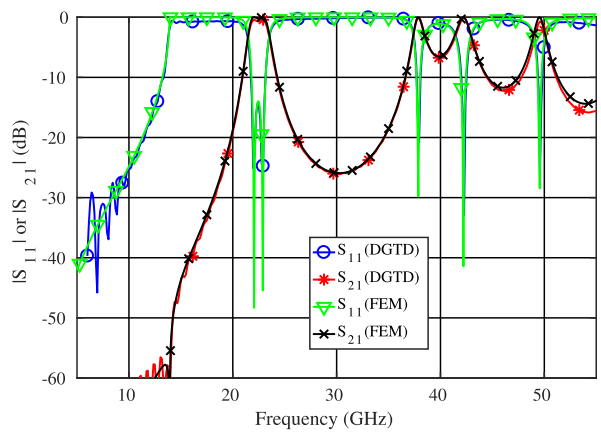

Fig. 12. S-parameters of the dielectric-loaded waveguide filter.

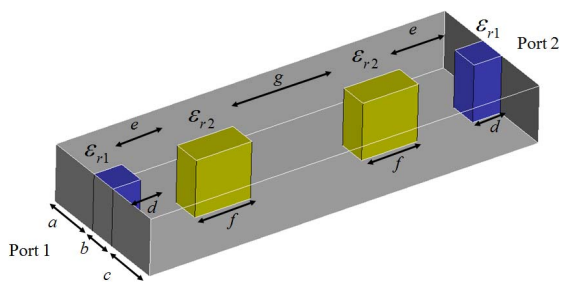

Fig. 11. Geometry of the dielectric-loaded waveguide filter [9]. The dielectric blocks at the ports have a relative permittivity of 9.7 and those inside have a relative permittivity of 7. The dimensions of the waveguide filter are $a = 2$, $b = 1$, $c = 2$, $d = 1$, $e = 2$, $f = 2$, and $g = 4$, all in mm.

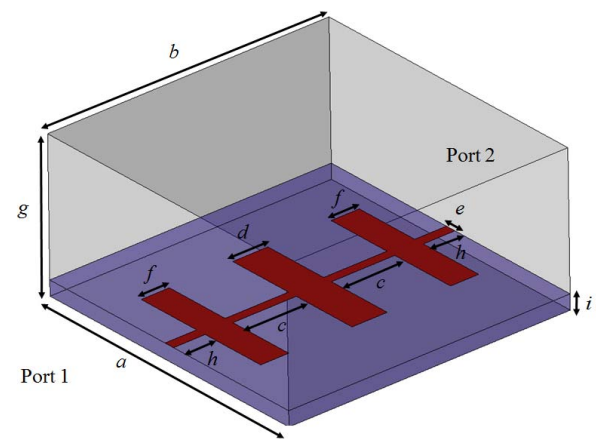

Fig. 13. Geometry of the microstrip low-pass filter. The substrate has a permittivity of 12.7 and a thickness of 0.2 mm. The dimensions of the waveguide are $a = 4$, $b = 4$, $c = 0.9$, $d = 0.5$, $e = 0.143$, $f = 0.4$, $g = 2$, $h = 0.45$, and $i = 0.2$, all in mm.

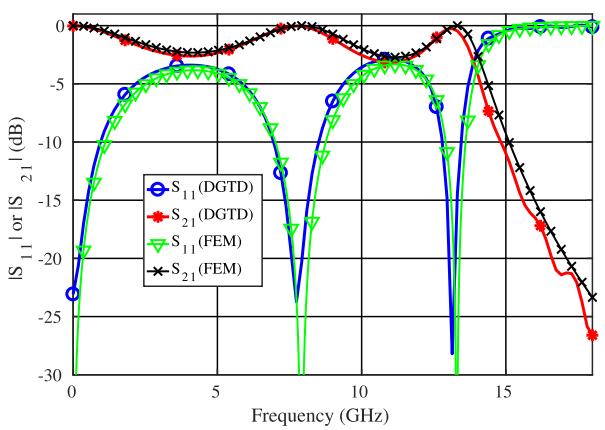

Fig. 14. S-parameters of the microstrip low-pass filter.

This waveguide filter is simulated over a very wide frequency band from 5 to 55 GHz. For this, the first mode computed at 35 GHz is used to excite the waveport with eight-layer PML on each port. The S-parameters of the waveguide filter are shown in Fig. 12, where the results from the proposed method are compared with the ones obtained by using the frequency-domain FEM solver in ANSYS HFSS. Good agreement is observed for the entire frequency range, showing that the proposed method is also applicable to devices with inhomogeneous waveports. It should be noted that the S-parameters below the cutoff frequency of 14 GHz are accurately extracted by the proposed scheme, which is a difficult task for most time-domain methods.

E. Microstrip Low-Pass Filter

The next example is a microstrip low-pass filter shown in Fig. 13. As shown, the filter is comprised of a staggered microstrip line, a substrate, and a rectangular waveguide. The microstrip line is printed on a substrate, which has a relative permittivity of 12.7 and a thickness of 0.2 mm. The substrate is placed in the bottom of the rectangular waveguide. In this simulation, the first mode, which is a quasi-TEM mode, calculated at the central frequency of 9 GHz is used to excite the waveport. To truncate the waveport, eight-layer PML is placed behind each port. The calculated S-parameters are shown in Fig. 14, which demonstrates good agreement between the results from the DGTD and the frequency-domain FEM solver supplied by CST STUDIO Suite.

F. Miniature Ridge Waveguide Filter

The last example is a miniature ridge waveguide bandpass filter operating in the frequency band of 6 to 8.6 GHz [32],

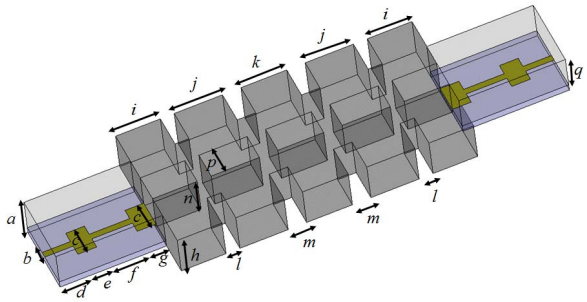

Fig. 15. Geometry of the miniature ridge-waveguide filter [32]. The dimensions of the waveguide are $a = 1.5$, $b = 0.22$, $c = 1$, $d = 1$, $e = 0.66$, $f = 1.425$, $g = 0.66$, $h = 1.5$, $i = 1.57$, $j = 1.695$, $k = 1.61$, $l = 0.49$, $m = 0.65$, $n = 1.375$, and $q = 1.246$, all in mm.

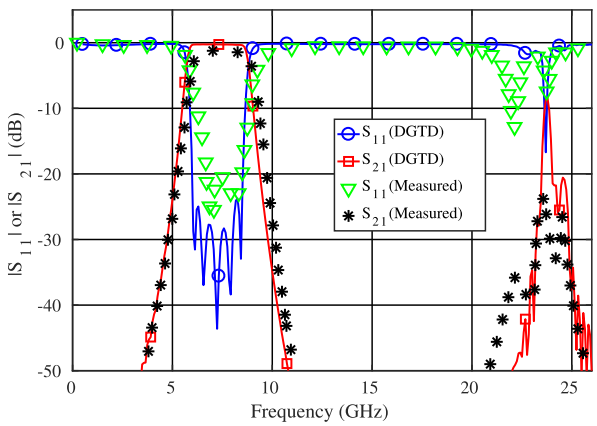

Fig. 16. S-parameters of the miniature ridge waveguide filter.

as shown in Fig. 15. The cavities in the filter are filled with a high dielectric constant material with $\varepsilon_r = 9.5$ and $\sigma = 0.002$ S/m. The impedance matching circuit is built on an alumina substrate, whose relative permittivity and conductivity are $\varepsilon_r = 10$ and $\sigma = 0.002$ S/m, respectively. Here, we use an eight-layer PML to truncate the waveport and employ third-order basis functions with 2447 tetrahedral elements and 344 wedge elements used in physical and PML regions, respectively. The simulated S-parameters, as shown in Fig. 16, are compared with the measurement, showing again good agreement. Note that this example was simulated previously in [17] using a PML and lumped element excitation. To obtain accurate results, the microstrip lines at the input and output ports had to be extended to a certain distance. No such extension is, however, needed in the current proposed method.

VI. Conclusion

A general numerical scheme was proposed for the waveport modeling and S-parameter extraction of inhomogeneous waveports with the DGTD method. In this scheme, the waveports were truncated with PMLs with a hybrid mesh automatically extruded from the mesh of the physical device to be simulated. The waveports were then excited by a TF/SF technique, with which the incident and scattered waves can be obtained for an accurate calculation of the S-parameters. A novel eigenmode solver was also developed to calculate the modal profiles for the eigenmodes in both homogeneous and inhomogeneous waveports. Several numerical examples were presented to validate the proposed numerical scheme and demonstrate its capabilities.

References

[1] J. S. Hesthaven and T. Warburton, "Nodal high-order methods on unstructured grids: I. Time-domain solution of Maxwell's equations," *J. Comput. Phys.*, vol. 181, no. 1, pp. 186–221, 2002.

[2] T. Lu, P. Zhang, and W. Cai, "Discontinuous Galerkin methods for dispersive and lossy Maxwell's equations and PML boundary conditions," *J. Comput. Phys.*, vol. 200, no. 2, pp. 549–580, Nov. 2004.

[3] B. Cockburn, F. Li, and C.-W. Shu, "Locally divergence-free discontinuous Galerkin methods for the Maxwell equations," *J. Comput. Phys.*, vol. 194, no. 2, pp. 588–610, Mar. 2004.

[4] L. Fezoui, S. Lanteri, S. Lohrengel, and S. Piperno, "Convergence and stability of a discontinuous Galerkin time-domain method for the 3D heterogeneous Maxwell equations on unstructured meshes," *ESAIM, Math. Model. Numer. Anal.*, vol. 39, no. 6, pp. 1149–1176, 2005.

[5] E. Montseny, S. Pernet, X. Ferriéres, and G. Cohen, "Dissipative terms and local time-stepping improvements in a spatial high order discontinuous Galerkin scheme for the time-domain Maxwell's equations," *J. Comput. Phys.*, vol. 227, no. 14, pp. 6795–6820, 2008.

[6] S. Gedney *et al.*, "The discontinuous Galerkin finite-element time-domain method solution of Maxwell's equations," *J. Appl. Comput. Electromagn. Soc.*, vol. 24, no. 2, pp. 129–142, 2009.

[7] K. Ise, K. Inoue, and M. Koshiba, "Three-dimensional finite-element solution of dielectric scattering obstacles in a rectangular waveguide," *IEEE Trans. Microw. Theory Techn.*, vol. 38, no. 9, pp. 1352–1359, Sep. 1990.

[8] J. Liu, J.-M. Jin, E. K. N. Yung, and R. S. Chen, "A fast, higher order three-dimensional finite-element analysis of microwave waveguide devices," *Microw. Opt. Technol. Lett.*, vol. 32, no. 5, pp. 344–352, 2002.

[9] W. K. Gwarek and M. Celuch-Marcysiak, "Wide-band S-parameter extraction from FD-TD simulations for propagating and evanescent modes in inhomogeneous guides," *IEEE Trans. Microw. Theory Techn.*, vol. 51, no. 8, pp. 1920–1928, Aug. 2003.

[10] D.-K. Sun, J.-F. Lee, and Z. Cendes, "The transfinite-element time-domain method," *IEEE Trans. Microw. Theory Techn.*, vol. 51, no. 10, pp. 2097–2105, Oct. 2003.

[11] T. Rylander and J.-M. Jin, "Stable coaxial waveguide-port algorithm for the time-domain finite-element method," *Microw. Opt. Technol. Lett.*, vol. 42, no. 2, pp. 115–119, 2004.

[12] T.-H. Loh and C. Mias, "Implementation of an exact modal absorbing boundary termination condition for the application of the finite-element time-domain technique to discontinuity problems in closed homogeneous waveguides," *IEEE Trans. Microw. Theory Techn.*, vol. 52, no. 3, pp. 882–888, Mar. 2004.

[13] Z. Lou and J.-M. Jin, "An accurate waveguide port boundary condition for the time-domain finite-element method," *IEEE Trans. Microw. Theory Techn.*, vol. 53, no. 9, pp. 3014–3023, Sep. 2005.

[14] C. Potratz, H.-W. Glock, and U. van Rienen, "Time-domain field and scattering parameter computation in waveguide structures by GPU-accelerated discontinuous-Galerkin method," *IEEE Trans. Microw. Theory Techn.*, vol. 59, no. 11, pp. 2788–2797, Nov. 2011.

[15] F. G. Hu and C. F. Wang, "Modeling of waveguide structures using DG-FETD method with higher order tetrahedral elements," *IEEE Trans. Microw. Theory Techn.*, vol. 60, no. 7, pp. 2046–2054, Jul. 2012.

[16] J. Alvarez, L. Angulo, A. R. Bretones, and S. G. Garcia, "A spurious-free discontinuous Galerkin time-domain method for the accurate modeling of microwave filters," *IEEE Trans. Microw. Theory Techn.*, vol. 60, no. 8, pp. 2359–2369, Aug. 2012.

[17] C.-P. Chang, G. Chen, S. Yan, and J. Jin, "Waveport modeling for the DGTD simulation of electromagnetic devices," *Int. J. Numer. Model. Electron. Netw., Devices Field*, 2017. [Online]. Available: https://doi.org/10.1002/jnm.2226

[18] P. Li, L. J. Jiang, and H. Bağci, "Transient analysis of dispersive power-ground plate pairs with arbitrarily shaped antipads by the DGTD method with wave port excitation," *IEEE Trans. Electromagn. Compat.*, vol. 59, no. 1, pp. 172–183, Feb. 2017.

[19] L. Zhao, G. Chen, W. Yu, and J.-M. Jin, "A fast waveguide port parameter extraction technique for the DGTD method," *IEEE Antennas Wireless Propag. Lett.*, vol. 16, pp. 2659–2662, 2017.

[20] R. Holland and J. W. Williams, "Total-field versus scattered-field finite-difference codes: A comparative assessment," *IEEE Trans. Nucl. Sci.*, vol. NS-30, no. 6, pp. 4583–4588, Dec. 1983.

[21] D. J. Riley, J.-M. Jin, Z. Lou, and L. E. R. Petersson, "Total-and scattered-field decomposition technique for the finite-element time-domain method," *IEEE Trans. Antennas Propag.*, vol. 54, no. 1, pp. 35–41, Jan. 2006.

[22] J. Alvarez, L. D. Angulo, M. F. Pantoja, A. R. Bretones, and S. G. Garcia, "Source and boundary implementation in vector and scalar DGTD," *IEEE Trans. Antennas Propag.*, vol. 58, no. 6, pp. 1997–2003, Jun. 2010.

[23] J.-M. Jin, *The Finite Element Method in Electromagnetics*, 3rd ed. Hoboken, NJ, USA: Wiley, 2014.

[24] A. Taflove and S. C. Hagness, *Computational Electrodynamics: The Finite-Difference Time-Domain Method*, 3rd ed. Norwood, MA, USA: Artech house, 2005.

[25] G. Cohen, X. Ferrieres, and S. Pernet, "A spatial high-order hexahedral discontinuous Galerkin method to solve Maxwell's equations in time domain," *J. Comput. Phys.*, vol. 217, no. 2, pp. 340–363, Sep. 2006.

[26] R. B. Lehoucq, D. C. Sorensen, and C. Yang, *ARPACK Users' Guide: Solution of Large-Scale Eigenvalue Problems With Implicitly Restarted Arnoldi Methods*. Philadelphia, PA, USA: SIAM, 1998.

[27] J.-M. Jin, *Theory and Computation of Electromagnetic Fields*, 2nd ed. Hoboken, NJ, USA: Wiley, 2015.

[28] J. G. Maloney, G. S. Smith, and W. R. Scott, "Accurate computation of the radiation from simple antennas using the finite-difference time-domain method," *IEEE Trans. Antennas Propag.*, vol. 38, no. 7, pp. 1059–1068, Jul. 1990.

[29] R. H. Sheikh and M. W. Gunn, "Wave propagation in a rectangular waveguide inhomogeneously filled with semiconductors," *IEEE Trans. Microw. Theory Techn.*, vol. MTT-16, no. 2, pp. 117–121, Feb. 1968.

[30] F. E. Gardiol, "Higher-order modes in dielectrically loaded rectangular waveguides," *IEEE Trans. Microw. Theory Techn.*, vol. MTT-16, no. 11, pp. 919–924, Nov. 1968.

[31] D. Baumann, C. Fumeaux, and R. Vahldieck, "Field-based scattering-matrix extraction scheme for the FVTD method exploiting a flux-splitting algorithm," *IEEE Trans. Microw. Theory Techn.*, vol. 53, no. 11, pp. 3595–3605, Nov. 2005.

[32] C. Rauscher and S. W. Kirchoefer, "Miniature ridge-waveguide filter module employing moldable dielectric material," *IEEE Trans. Microw. Theory Techn.*, vol. 54, no. 3, pp. 1190–1195, Mar. 2006.

Geng Chen was born in Suqian, China, in 1989. He received the B.S. and M.S. degrees in computational mathematics from Jiangsu Normal University, Xuzhou, China, in 2012 and 2015, respectively.

From 2015 to 2017, he was with the Department of Electrical and Computer Engineering, University of Illinois at Urbana–Champaign, Urbana, IL, USA, as a Visiting Scholar. He joined the National Supercomputing Center, Wuxi, China, in 2017. His current research interests include numerical methods in electromagnetics and wave propagation, hardware acceleration techniques, and software development.

Lei Zhao (M'09) received the B.S. degree in mathematics from Jiangsu Normal University, Xuzhou, China, in 1997, and the M.S. degree in computational mathematics and Ph.D. degree in electromagnetic fields and microwave technology from Southeast University, Nanjing, China, in 2004 and 2007, respectively.

From 2007 to 2009, he was with the Department of Electronic Engineering, The Chinese University of Hong Kong, Hong Kong, as a Research Associate. In 2011, he was with the Department of Electrical and Computer Engineering, National University of Singapore, Singapore, as a Research Fellow. From 2016 to 2017, he was with the Department of Electrical and Computer Engineering, University of Illinois at Urbana–Champaign, Urbana, IL, USA, as a Visiting Scholar. He joined Jiangsu Normal University, in 2009, where he is currently the Associate Director of the Jiangsu Key Laboratory of Education Big-Data Science and Engineering and the Vice Dean of the School of Mathematics and Statistics. He has authored or co-authored over 40 referred journal and conference papers. His current research interests include computational electromagnetics, bioelectromagnetics, and millimeter-wave components, including filters and antenna arrays.

Dr. Zhao is a member of the Applied Computational Electromagnetics Society. He serves as a Reviewer for multiple journals and conferences, including IEEE ANTENNAS AND WIRELESS PROPAGATION LETTERS, IEEE ACCESS, *Progress in Electromagnetics Research*, and the *Applied Computational Electromagnetics Society Journal*. He also serves as a Lead Guest Editor of the *Applied Computational Electromagnetics Society Journal*.

Wenhua Yu (M'99–SM'00) is currently a Professor with Jiangsu Normal University, Xuzhou, China, where he is also the Director of the Jiangsu Key Laboratory of Education Big-Data Science and Engineering. Before joining JSNU, he was the President of 2COMU, Fairfax, VA, USA, and a Professor with the Electrical Engineering Department, Pennsylvania State University, State College, PA, USA. His current research interests include CEM, FDTD, hardware acceleration technology, and big data.

Su Yan (S'08–M'12–SM'17) received the B.S. degree in electromagnetics and microwave technology from the University of Electronic Science and Technology of China, Chengdu, China, in 2005, and the M.S. and Ph.D. degrees in electrical and computer engineering from the University of Illinois at Urbana–Champaign, Urbana, IL, USA, in 2012 and 2016, respectively.

He is currently a Post-Doctoral Research Associate with the Department of Electrical and Computer Engineering, University of Illinois at Urbana–Champaign, and has been appointed as an Instructor in 2012 and since 2016. He has authored or co-authored over 90 papers in refereed journals and conferences. His current research interests include nonlinear electromagnetic and multiphysics problems, electromagnetic scattering and radiation, numerical methods in computational electromagnetics, especially FEMs, integral equation-based methods, fast algorithms, and preconditioning techniques.

Dr. Yan is a member of the Applied Computational Electromagnetics Society (ACES). He was a recipient of the Best Student Paper Award of the IEEE Chengdu Section in 2010, the Best Student Paper Award (the First Place Winner) of the 27th International Review of Progress in the ACES, Williamsburg, VA, USA, in 2011, the USNC/URSI Travel Fellowship Grant Award of the National Academies in 2015, the Best Student Paper Award (the First Place Winner) of the IEEE ICWITS/ACES 2016 Conference, Honolulu, HI, USA, in 2016, and the Yuen T. Lo Outstanding Research Award and the P. D. Coleman Outstanding Research Award of the Department of Electrical and Computer Engineering, University of Illinois at Urbana–Champaign, in 2014 and 2015, respectively. He serves as a Reviewer for multiple journals and conferences, including the PROCEEDINGS OF THE IEEE, *IEEE Antennas and Propagation Magazine*, the IEEE TRANSACTIONS ON ANTENNAS AND PROPAGATION, the IEEE TRANSACTIONS ON MICROWAVE THEORY AND TECHNIQUES, and the IEEE TRANSACTIONS ON MAGNETICS. He also serves as a Lead Guest Editor of the *International Journal of Antennas and Propagation*. His name appeared in the University of Illinois at Urbana–Champaign's List of Teachers Ranked as Excellent by Their Students in 2012 with an outstanding rating (top 10%).

Kedi Zhang (S'13–M'17) received the B.S. degree in electrical engineering from the University of Electronic Science and Technology of China, Chengdu, China, in 2009, and the M.S. degree in electrical engineering from Southeast University, Nanjing, China, in 2012. He is currently pursuing the Ph.D. degree in electrical engineering at the University of Illinois at Urbana–Champaign, Urbana, IL, USA.

Since 2012, he has been a Research Assistant with the Center for Computational Electromagnetics, Department of Electrical and Computer Engineering, University of Illinois at Urbana–Champaign. His current research interests include numerical simulation of composite materials and microwave and millimeter-wave devices, generalized FEMs, fast boundary integral methods, domain decomposition methods, and parallel computing.

Mr. Zhang is a member of the Honor Society of Phi Kappa Phi. He was a recipient of the Computational Science and Engineering Fellowship presented by the University of Illinois at Urbana–Champaign in 2013 and 2014, the Raj Mittra Outstanding Graduate Research Award and the Professor Kung Chie Yeh Endowed Fellowship presented by the Department of Electrical and Computer Engineering, University of Illinois at Urbana–Champaign, in 2015 and 2016, respectively, and the USNC/URSI Travel Fellowship Grant Award from National Academies in 2015. He serves as a Reviewer for multiple journals, including the *Applied Computational Electromagnetics Society Journal*, the *International Journal of Numerical Modeling: Electronic Networks, Devices, and Fields*, and the IEEE TRANSACTIONS ON ANTENNAS AND PROPAGATION.

Jian-Ming Jin (S'87–M'89–SM'94–F'01) received the Ph.D. degree in electrical engineering from the University of Michigan, Ann Arbor, MI, USA, in 1989.

He joined the University of Illinois at Urbana–Champaign, Urbana, IL, USA, in 1993, where he is currently the Y. T. Lo Chair Professor of electrical and computer engineering and the Director of the Electromagnetics Laboratory and the Center for Computational Electromagnetics. He was appointed as the first Henry Magnuski Outstanding Young Scholar with the Department of Electrical and Computer Engineering in 1998 and later as a Sony Scholar in 2005. He was appointed as a Distinguished Visiting Professor with the Air Force Research Laboratory in 1999. He has been an Adjunct Professor, a Visiting Professor, a Guest Professor, and a Chair Professor for 11 universities worldwide. He has authored or co-authored over 250 papers in refereed journals and 22 book chapters. He has also authored *The Finite Element Method in Electromagnetics* (Wiley, First Edition 1993, Second Edition 2002, and Third Edition 2014), *Electromagnetic Analysis and Design in Magnetic Resonance Imaging* (CRC, 1998), and *Theory and Computation of Electromagnetic Fields* (Wiley, First Edition 2010 and Second Edition 2015), and co-authored *Computation of Special Functions* (Wiley, 1996), *Fast and Efficient Algorithms in Computational Electromagnetics* (Artech House, 2001), and *Finite-Element Analysis of Antennas and Arrays* (Wiley, 2008). His current research interests include computational electromagnetics, scattering and antenna analysis, electromagnetic compatibility, high-frequency circuit modeling and analysis, bioelectromagnetics, and magnetic resonance imaging. He was elected by ISI as one of the world's most cited authors in 2002.

Dr. Jin is a Fellow of the Electromagnetics Academy and Applied Computational Electromagnetics Society (ACES) and a member of URSI Commission B. He was a recipient of the 1994 National Science Foundation Young Investigator Award, the 1995 Office of Naval Research Young Investigator Award, the 1999 ACES Valued Service Award, the 2014 ACES Technical Achievement Award, the 2016 ACES Computational Electromagnetics Award, the 2015 IEEE Antennas and Propagation Society Chen-To Tai Distinguished Educator Award, the 2015 IEEE Antennas and Propagation Edward E. Altschuler AP-S Magazine Prize Paper Award, and the 1997 Xerox Junior Research Award and the 2000 Xerox Senior Research Award presented by the College of Engineering, University of Illinois at Urbana–Champaign. His name appeared 22 times in the University of Illinois at Urbana–Champaign's List of Excellent Instructors. His students have won the Best Paper Award of the IEEE 16th Topical Meeting on Electrical Performance of Electronic Packaging and 25th, 27th, 31st, and 32nd Annual Review of Progress in Applied Computational Electromagnetics. He served as an Associate Editor and the Guest Editor for the IEEE TRANSACTIONS ON ANTENNAS AND PROPAGATION, *Radio Science, Electromagnetics, Microwave and Optical Technology Letters*, and *Medical Physics.*